Mechanism of an ATP-Dependent Carboxylase, Dethiobiotin Synthetase, Based on Crystallographic Studies of Complexes with Substrates and a Reaction Intermediate†

Weijun Huang,‡ Jia Jia,‡ Katharine J. Gibson,§ Wendy S. Taylor,|| Alan R. Rendina,|| Gunter Schneider,*,‡ and Ylva Lindqvist*,‡

Department of Molecular Biology, Swedish University of Agricultural Sciences, Uppsala Biomedical Center, Box 590, S-75124 Uppsala, Sweden, Dupont Central Research and Development, Experimental Station, P.O. Box 80402, Wilmington, Delaware 19880-0402, and Dupont Agricultural Products, Stine-Haskell Research Center, P.O. Box 30, Newark, Delaware 19714-0030

Received March 16, 1995; Revised Manuscript Received May 24, 1995⊗

ABSTRACT: The crystal structures of six complexes of homodimeric *Escherichia coli* dethiobiotin synthetase with a variety of substrates, substrate analogs, and products have been determined to high resolution. These include (1) the binary complex of dethiobiotin synthetase and the N7-carbamate of 7,8-diaminononanoic acid, (2) the binary complex of enzyme and the alternate substrate, 3-(1-aminoethyl)-nonanedioic acid, (3) the binary complex of enzyme with the product ADP, (4) the quaternary complex of enzyme, ADP, the N7-carbamate of 7,8-diaminononanoic acid, and Ca^{2+}, (5) the ternary complex of enzyme, the ATP analog adenylyl (β,γ-methylene)diphosphonate, and the N7-carbamate of 7,8-diaminononanoic acid, and (6) the quaternary complex of enzyme, the ATP analog adenylyl (β,γ-methylene)diphosphonate, 7,8-diaminononanoic acid, and Mn^{2+}. One molecule of each substrate binds to one monomer of the enzyme. ADP and the ATP analogue bind to the classical mononucleotide binding fold with the phosphate groups close to the phosphate binding loop Gly8−Thr16 between β-strand β1 and the N-terminus of α-helix α1. The adenine ring is bound in a pocket between β-strands β6 and β7. In the quaternary complex with Mn^{2+}, the metal binding site is found in the vicinity of the β- and γ-phosphate groups. Two oxygen atoms from the phosphates and oxygen atoms from the side chains of Asp54, Thr16, and Glu115 are ligands to the Mn^{2+} ion in the quaternary complex. In the complex with ADP and the N7-carbamate of 7,8-diaminononanoic acid prepared in the presence of Ca^{2+} ions, a different metal binding site is found. The Ca^{2+} ion is coordinated to an oxygen atom of the α-phosphate group of the nucleotide, the side chain of Asp54, and solvent molecules. The 7,8-diaminononanoic acid substrate molecule interacts with residues from both subunits, making the dimer the minimal functional unit. The diamino group binds between the loops after β2 and β4, and the terminal carboxyl group at the hydrophobic tail of the substrate interacts with the amino terminus of helix α5 and with the side chain of Tyr187 in helix α6 of the second subunit at the monomer−monomer interface. Strong additional electron density close to the N7 nitrogen atom of the 7,8-diaminononanoic acid substrate in some complexes indicates that, even in the absence of added bicarbonate in the crystallization mixture, the carbamylated intermediate is formed in the crystal. The crystal structure of the binary complex of DTBS with the analog 3-(1-aminoethyl)nonanedioic acid is identical to that of the binary complex with substrate, providing further evidence that the true reaction intermediate has formed in these crystals. The overall structures of the native enzyme and the enzyme in the six complexes are very similar. However, binding of the substrate and the mononucleotide causes local conformational changes of loop regions close to the active site. On the basis of the crystal structures of these complexes, a reaction mechanism for dethiobiotin synthetase is proposed.

Dethiobiotin synthetase (DTBS)[1] is the penultimate enzyme in the biotin biosynthesis pathway in *Escherichia coli* and other microorganisms (Krell & Eisenberg, 1970). The enzyme catalyzes formation of the ureido ring of dethiobiotin from (7*R*,8*S*)-7,8-diaminononanoic acid (DAPA) and carbon dioxide (Figure 1). The enzyme utilizes carbon dioxide instead of hydrogen carbonate as substrate and is dependent on ATP and divalent metal ions as cofactors (Krell & Eisenberg, 1970). DTBS represents a third mechanistic solution to enzymatic carboxylation reactions, with the biotin-dependent carboxylases and ribulose bisphosphate carboxylase utilizing two other, different carboxylation mechanisms.

Detailed mechanistic information on DTBS is scarce, and biochemical studies of the reaction mechanism and identification of possible reaction intermediates have only been resumed recently (Baxter et al., 1994; Baxter & Baxter, 1994). The first step in the reaction involves formation of

† This work was supported by a grant from the Swedish Agricultural Research Council.

* Corresponding authors.
‡ Swedish University of Agricultural Sciences.
§ Dupont Central Research and Development.
|| Dupont Agricultural Products.

⊗ Abstract published in *Advance ACS Abstracts,* August 1, 1995.

[1] Abbreviations: DTBS, dethiobiotin synthetase; DAPA, (7*R*,8*S*)-7,8-diaminononanoic acid; DAPA-$^{7N}CO_2$, DAPA carbamylated at the N7 amino nitrogen; DAPA-$^{8N}CO_2$, DAPA carbamylated at the N8 amino nitrogen; AEND, 3-(1-aminoethyl)nonanedioic acid; ADP, adenosine diphosphate; ATP, adenosine triphosphate; AMPPCP, adenylyl (β,γ-methylene)diphosphonate.

0006-2960/95/0434-10985$09.00/0

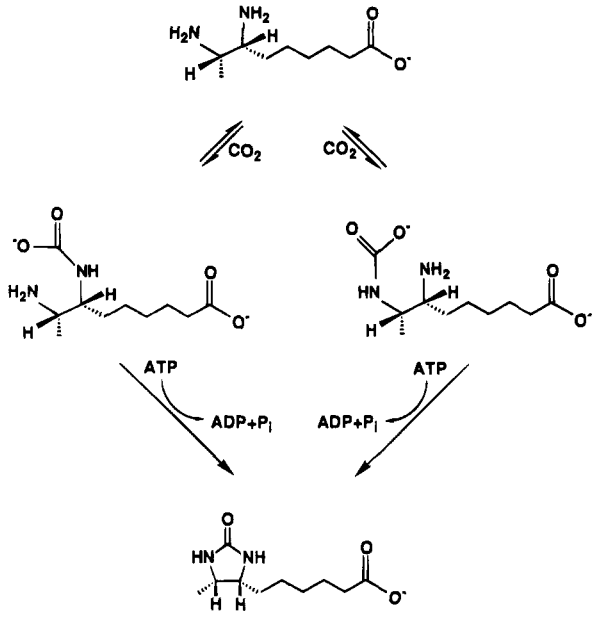

FIGURE 1: Scheme of the reaction catalyzed by dethiobiotin synthetase. Two alternative pathways, corresponding to carbamate formation at N7 or N8, respectively, are shown.

a carbamate of the substrate DAPA. In principle, carbamylation can occur on the N7 or N8 position of the substrate (Figure 1). In free solution, both carbamates of DAPA can be observed [see accompanying paper by Gibson et al. (1995)]. Trapping experiments suggested the N8-carbamate as the enzyme-bound reaction intermediate (Baxter et al., 1994). However, other biochemical evidence suggests that the N7-carbamate is the enzyme-bound intermediate (Gibson et al, 1995). The second step is the formation of an carbamic−phosphoric mixed anhydride as a second reaction intermediate (Baxter & Baxter, 1994), and the reaction concludes by ring closure, most likely through nucleophilic attack of a substrate nitrogen on the activated carbonyl group of the carbamate with release of inorganic phosphate.

The nucleotide sequences of DTBS from *E. coli* (Alexeev et al., 1994a), *Bacillus sphaericus* (Glöckler et al., 1990), *Brevibakterium flavum* (Hatakeyama et al., 1994), and *Serratia marcescens* (Sakurai, 1993) have been determined. Crystallographic studies of unliganded DTBS from *E. coli* (Huang et al., 1994) revealed that the three-dimensional structure of DTBS is similar to the structure of the GTP-dependent enzymes H-ras p21 protein (Pai et al., 1990) and adenylosuccinate synthetase (Poland et al., 1993). An independent crystallographic study of DTBS (Alexeev et al., 1994b) confirmed these results, and preliminary data on the binding of substrate to the active site were given; however, no details of the interactions of the substrate with the protein were reported. We have now extended our structural studies to binary, ternary, and quaternary complexes of the enzyme and report here the structure of DTBS complexed with its substrate, DAPA, an analogue of the reaction intermediate, AEND (Figure 2) or ADP, respectively, and the structures of the ternary complexes DTBS·ADP·DAPA and finally DTBS·AMPPCP·DAPA in the presence of Ca^{2+} or Mn^{2+} ions, respectively. These structural studies reveal residues involved in cofactor and substrate binding and suggest enzymatic groups which might be important for catalysis. We also present crystallographic evidence that carbamylation occurs at the N7 nitrogen atom of the substrate, an observation which is in conflict to chemical trapping experiments leading to the proposal of the N8 nitrogen atom as the site of carbamylation (Baxter & Baxter, 1994).

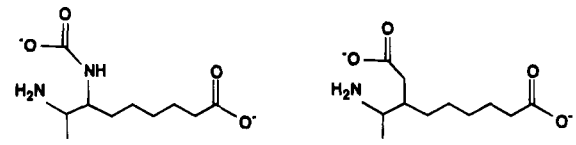

FIGURE 2: The reaction intermediate 7,8-diaminononanoic acid carbamylated at the N7 amino nitrogen (DAPA-$^{7N}CO_2$) and its analog, 3-(1-aminoethyl)nonanedioic acid (AEND).

MATERIALS AND METHODS

Materials. Purification of DTBS from an overexpressing strain of *E. coli* and the chemical synthesis of DAPA and AEND are described by Gibson et al. (1995). ADP and AMPPCP were purchased from Boehringer Mannheim (Germany).

Crystallization. Native crystals of DTBS were obtained as described by Huang et al. (1994) with poly(ethylene glycol) as precipitant. Crystals of the complexes with DAPA or AEND were prepared by cocrystallization of native enzyme in the presence of 5 mM DAPA or AEND, respectively, and of either 200 mM $CaCl_2$ or 100 mM $MnCl_2$ or by soaking native crystals in the crystallizing reservoir solution containing 5 mM DAPA. Crystals of the DTBS·ADP complex were prepared by soaking native crystals in the crystallizing reservoir solution containing 5 mM ADP. The complexes DTBS·ADP·DAPA, DTBS·AMPPCP·DAPA, and DTBS·AMPPCP·DAPA were prepared by soaking DTBS·DAPA crystals obtained by cocrystallization with 5 mM ADP or AMPPCP, respectively, in the presence of either 200 mM $CaCl_2$ or 100 mM $MnCl_2$. Crystals of these complexes are isomorphous to the native crystals, space group C_2, with cell dimensions $a = 73.2$ Å, $b = 49.2$Å, $c = 61.8$Å, and $\beta = 107.1°$.

Data Collection. Diffraction data sets were collected on an *R*-axis imaging plate, and the images were processed with the MSC software (Sato et al., 1992). One data set for the binary complex DTBS·DAPA was collected on a Xentronix multiwire area detector, and the frames were processed with Buddha (Blum et al., 1987). Details of the data collection are given in Table 1.

Model Building and Crystallographic Refinement. Difference Fourier methods were used to solve the structures of the complexes of DTBS. Crystallographic calculations were carried out with the CCP4 program package (Collaborative Computational Project, Number 4, 1994). Initial phases were calculated from the coordinates of the refined, unliganded enzyme, which at present has a crystallographic *R*-factor of 16.9% at 1.65 Å resolution (Huang et al., 1994). Water molecules near the active site were excluded from the initial structure factor calculations.

Model building was carried out with the program O (Jones et al., 1991), and crystallographic refinement was carried out using X-PLOR (Brünger et al., 1987). Before any substrate modeling was done, conventional positional refinement by energy minimization was performed. Difference electron density maps calculated from these coordinates were then used to model substrate molecules. Water molecules with temperature factors higher than 60 Å^2 or with ill-defined electron density were deleted from the model, and new water

Table 1: Details of Crystallographic Data Collection and Refinement

complex	DAPA-1[a]	DAPA-2[b]	DAPA-3[c]	AEND	ADP	DAPA·ADP	DAPA·AMPPCP	DAPA·AMPPCP·Mn^{2+}
resolution (Å)	1.70	2.00	1.70	1.70	1.60	1.70	1.64	1.64
no.. of measured reflections	51918	22161	50706	60324	91245	52543	61271	38766
no. of unique reflections	20598	13280	20347	23576	25367	21243	22267	19323
completeness of X-ray data (%)	90	93	88	95	87	93	87	75
R_{merge}[d]	0.070	0.037	0.074	0.050	0.051	0.059	0.059	0.079
no. of residues in the model	220	220	220	220	224	224	224	224
no. of non-hydrogen protein atoms in the final model	1651	1651	1651	1651	1692	1692	1692	1692
no. of solvent atoms	162	183	151	183	166	200	199	187
R-factor (%)	17.1	19.9	17.8	17.3	18.3	17.2	18.0	17.4
mean temperature factors								
protein atoms (Å^2)	22.5	18.2	24.1	20.9	25.8	21.9	22.7	20.3
solvent atoms (Å^2)	38.3	36.4	37.2	38.6	40.0	34.1	36.8	36.7
substrate atoms (Å^2)	28.9	31.6	28.8	28.0	35.3	22.7	36.0	34.9
rms bond deviations (Å)	0.014	0.019	0.014	0.014	0.014	0.014	0.016	0.013
rms angle deviations (deg)	2.7	2.9	2.7	2.7	2.6	2.6	2.7	2.7
rms dihedral deviations (deg)	23.9	24.4	24.1	24.0	24.5	24.2	24.5	24.6
rms improper deviations (deg)	1.8	1.6	1.8	1.6	1.7	1.6	1.5	1.8
Ramachandran plot								
no. of non-glycine residues in unfavorable (disallowed) regions	0 (0)	1 (1)	0 (0)	1 (0)	0 (0)	0 (0)	0 (0)	0 (0)

[a] Cocrystallized in the presence of 5 mM DAPA and 200 mM $CaCl_2$. [b] Native crystals soaked with 5 mM DAPA in the presence of 200 mM $CaCl_2$. [c] Cocrystallized in the presence of 100 mM $MnCl_2$. [d] $R_{merge} = \sum\sum_i|I_i - \langle I\rangle|/\sum|\langle I\rangle|$, where I_i are the intensity measurements for a reflection and $\langle I\rangle$ is the mean value for the reflection.

molecules were added where indicated. Crystallographic R-factors for the different data sets usually were around 25% before refinement and dropped to around 18% while maintaining good stereochemistry after a few rounds of modeling and refinement. Details of the refinement statistics are given in Table 1. The models of all complexes were analyzed with PROCHECK (Laskowski et al., 1993). The atomic coordinates of the DTBS complexes have been deposited with the Brookhaven Protein Data Bank.[2]

Structure Comparisons. The structures of DTBS complexes were compared with the structures of p21 complexed with the GTP analog guanosine 5′-(β,γ-imido)triphosphate (Pai et al., 1990, PDB accession code 5P21) and adenylate kinase complexed with its inhibitor Ap5A (Müller & Schulz, 1992, PDB entry 1AKE) using the LSQ options in O (Jones et al., 1991).

RESULTS

Electron Density Maps and Overall Structures. As can be seen from Table 1, crystallographic refinement of the binary and ternary complexes of DTBS resulted in well-refined protein models. No outliers (except glycine residues) in the disallowed regions of the Ramachandran plot were found. The electron density for the polypeptide chain and amino acid side chains is well defined in all the complexes except a few regions (see below).

The overall structure of the enzyme in the complexes is similar to the structure of the free enzyme, indicating that no large conformational changes occur upon binding of the substrates. The overall rms deviations for 219 Cα atoms (residues 208−212 were not included in the comparison, since they are disordered in the free enzyme and the enzyme−DAPA complex) between the native enzyme and the complexes are 0.30 Å (DTBS·DAPA), 0.38 Å (DTBS·AEND), 0.33 Å (DTBS·ADP), 0.49 Å (DTBS·ADP·DAPA·Ca^{2+}), 0.43 Å (DTBS·AMPPCP·DAPA), and 0.43 Å (DTBS·AMPPCP·DAPA·Mn^{2+}). Figure 3 shows the rms deviations of these 219 Cα atoms as a function of residue number. Significant residue displacements occur in a few localized regions of the polypeptide chain. One of these regions is the phosphate binding loop between β1 and α1, residues 9−14, which changes conformation upon binding of the ATP analog or ADP. To a lesser extent, this loop also changes its conformation upon binding of DAPA or AEND. The next region with significant shifts are residues 117−119 in the loop after β strand β4, involved in binding of DAPA and interacting with the phosphate binding loop. Another significant conformational change occurs at the region around residue 146−152 in the loop after β5, which also is close to the phosphate binding loop. This loop is directly involved in subunit−subunit interactions of the homodimer and binds to the carboxyl group of the DAPA substrate in the dimer. Another region of the polypeptide chain displaying significant shifts in the atomic positions compared to the native enzyme comprises residues 208−212. In the native enzyme and the binary complex with DAPA, this loop is disordered in the crystals. In the complexes with nucleotides, Glu211 forms a hydrogen bond to a nitrogen of the adenine ring, and residue Pro210 forms a hydrophobic interaction with

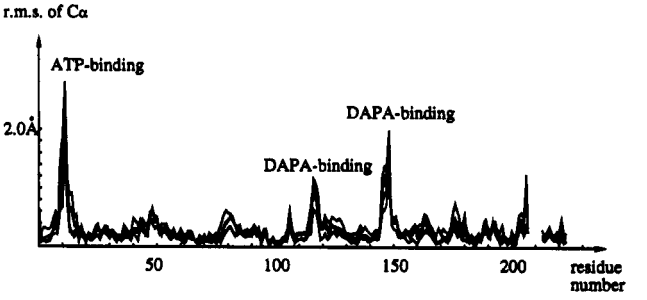

FIGURE 3: rms deviations of Cα atoms as a function of residue number for the enzyme complexes after superposition onto the structure of the free enzyme.

[2] The entry numbers for the atomic coordinates of the DTBS complexes at the Brookhaven Protein Data Bank are as follows: DTBS·DAPA, 1DAF; DTBS·AEND, 1DAE; DTBS·ADP, 1DAD; DTBS·ADP·DAPA, 1DAI; DTBS·AMPPCP·DAPA, 1DAG; and DTBS·AMPPCP·DAPA·Mn^{2+}, 1DAH.

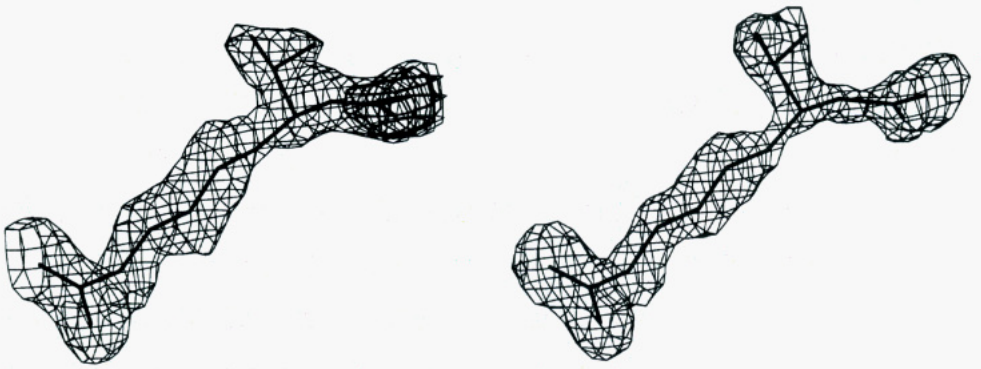

FIGURE 4: Difference electron density for bound substrates in various DTBS·substrate complexes. (a, left) Part of an $|F_o| - |F_c|$ map of the DTBS·DAPA complex. The difference electron density (contoured at 2 times the standard deviation of the electron density map, thin lines) for the refined model of DAPA-$^{7N}CO_2$ is shown. Structure factors were calculated after refinement of the DTBS·DAPA-$^{7N}CO_2$ complex but with the substrate atoms excluded from the structure factor calculation. Thick lines represent residual electron density close to the position of the N7 amino group (contoured at 3.5 times the standard deviation of the electron density map) found when only a model of a noncarbamylated DAPA molecule is included in the crystallographic refinement of the DTBS·DAPA complex. (b, right) Part of an $|F_o| - |F_c|$ map, showing the difference electron density for the bound analog of the reaction intermediate in the binary complex DTBS·AEND. Structure factors were calculated with atoms of the analog excluded in the calculation. The difference electron density is contoured at 2 times the standard deviation of the electron density map.

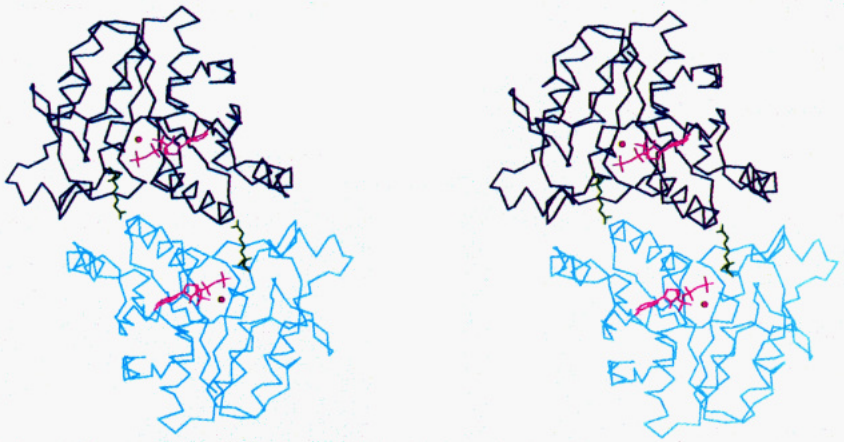

FIGURE 5: Overall view of the binding of DAPA-$^{7N}CO_2$ and the ATP analog to dethiobiotin synthetase. The Cα trace of the enzyme dimer is shown in different shades of blue to indicate the two subunits. Bound DAPA-$^{7N}CO_2$ is shown in green and the ATP analog in pink. The positions of the Mn^{2+} ions are indicated by red spheres.

the aromatic ring, resulting in a better defined loop conformation.

Binary Complexes DTBS·DAPA and DTBS·AEND. X-ray data from three enzyme−DAPA complexes, prepared by crystal soaking and cocrystallization, have been collected and refined independently. Comparison of these three models of the binary complex revealed that the structures are, within the error limits of the electron density map, identical. Furthermore, the overall structure of the binary complex is with few exceptions similar to the structure of the free enzyme, and we conclude that necessary conformational changes upon binding of substrate can be accommodated within the enzyme crystal. In the following discussions, the structure of the binary complex obtained by cocrystallization in the presence of Mn^{2+} ions will be used, although most features are observed in all three substrate complexes.

In the electron density maps, strong difference electron density was observed, stretching from the active site of one monomer to protein residues of the second subunit at the monomer−monomer interface. A model of DAPA could readily be built into this electron density, and due to the high resolution of the electron density maps, the orientation of the substrate could be determined with high confidence (Figure 4a).

In these electron density maps, strong electron density close to the N7 nitrogen atom of DAPA was found (Figure 4a). At the present resolution (1.70 Å), the best fit to this density is that of a carboxyl group. This would mean that the substrate in these crystals is of the carbamylated form and in fact represents the first reaction intermediate. Refinement of the model yields excellent electron density for the carbamylated substrate, and the temperature factors are similar to those of the other substrate atoms.

The substrate is bound at the switchpoint between β-strands β2 and β4, and residues from loop regions after the adjacent β-strands, β1 and β3, are also close to the substrate. DAPA forms hydrogen bonds with residues from both of the subunits in the homodimer, which suggests a dimer of DTBS as the catalytically competent unit. Figure 5 gives an overall view of the substrate binding sites in DTBS. The carboxyl group at the hydrophobic tail interacts with the amino terminus of helix α5; each of its oxygen atoms forms a hydrogen bond to the main-chain nitrogens of residues 150 and 153, respectively. One of the carboxyl oxygens forms an additional hydrogen bond to the side chain of Tyr187, which changes its position as a consequence of this new interaction (Figure 6). The second carboxyl oxygen forms an additional hydrogen bond to a water molecule. Due to

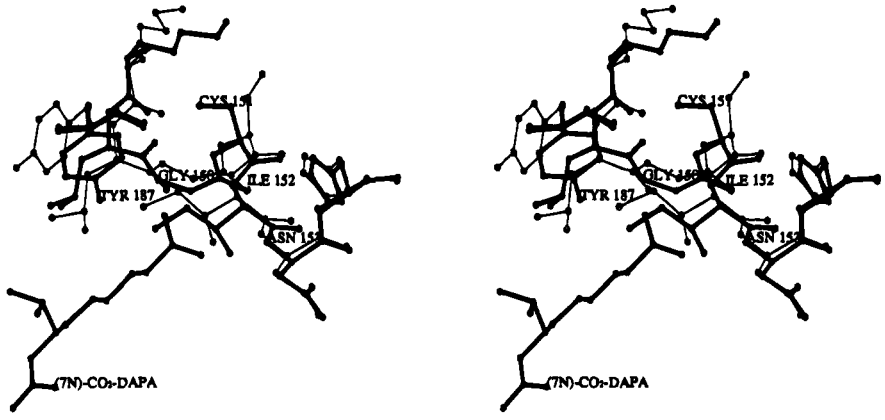

FIGURE 6: Stereoview illustrating the conformational changes at the subunit−subunit interface upon binding of DAPA-$^{7N}CO_2$ to dethiobiotin synthetase. Thin lines: native enzyme. Thick lines: DTBS·DAPA-$^{7N}CO_2$ complex.

the interactions of the substrate carboxyl group with the amino terminus of helix α5, local structural changes occur. The main-chain oxygen atom of residue 149 flips so that N150 can form a hydrogen bond with the substrate, and this peptide flip results in a slight change of the conformation of the loop after β5 and the terminus of the helix, comprising residues 146−152. Part of these structural changes is a change in the conformation of the side chain of Cys151. These conformational changes induce a shift in the phosphate binding loop so that it moves closer to the substrate in the other subunit.

The hydrophobic tail of the substrate spans the space between the subunit−subunit interface to the active site and packs against residues from the loops after strand β4 and strand β3. The diamino end of the substrate is bound at the switchpoint between the ends of strands β4 and β2. The N7 nitrogen atom forms a hydrogen bond to the side chain of Ser41, and the N8 nitrogen atom forms a hydrogen bond to a solvent molecule. These interactions are different from those reported by Alexeev et al. (1994b). On the basis of their unrefined structure with DAPA bound to the enzyme (however, at low occupancies and at lower resolution, 2.3 Å), the 7-amino group is reported to be close to residues Asp81 (which is a serine residue in the amino acid sequence) and Thr122. They find only the 8-amino group in the vicinity of the γ-phosphate group. In the complexes described here, both amino groups are close to the position of the γ-phosphate; the distance between the N7-amino group to the closest γ-phosphate oxygen atom is 2.9 Å and that of the N8-amino group 3.9 Å, respectively.

One of the carbamate oxygens makes an interaction via a solvent molecule to the side chain of Lys15 and is close (3.5 Å) to the side chain of Lys37. This oxygen atom is also within hydrogen-bonding distance to the N8 nitrogen of the substrate and could form an internal hydrogen bond. The second carbamate oxygen is held into place through a number of interactions including hydrogen bonds to the main-chain nitrogen and oxygen atoms of residue 41 and a solvent molecule.

The compound AEND is a stable mimic of this first reaction intermediate, DAPA-$^{7N}CO_2$, provided that the carbamylation indeed occurs at the N7 position of the substrate (Figures 1 and 2, Gibson et al., 1995). It is also an alternate substrate of the enzyme. In the electron density map of the binary complex of DTBS with AEND, strong electron density corresponding the bound analog was found (Figure 4b). This electron density corresponds in shape and location precisely to the electron density observed in the binary complex of the enzyme with DAPA. A model of the reaction intermediate could easily be fitted into this density (Figure 4b). Except for the hydrogen bond between N7 and the side chain of Ser41, the interactions of bound AEND with DTBS are otherwise identical to the interactions of the modeled true intermediate observed in the crystals with DAPA (see above), which further supports the assignment of the additional density in the DTBS·DAPA complex as that of a carboxyl group.

Enzyme·ADP Complex. The nucleotide is well defined in electron density. The adenine ring binds in a pocket formed by the ends of strands β6 and β7. The diphosphate group points toward the active site and is close to the phosphate binding loop formed by residues Gly8−Thr16 in the connecting loop between β1 and α1. The α-phosphate points to the N-terminal of helix α1. A stereoview of the ADP binding site in DTBS is given in Figure 7.

The nucleotide interacts with the enzyme directly through a number of hydrogen bonds and van der Waals contacts. Three nitrogen atoms of the adenine ring are engaged in hydrogen bonds, the N1 nitrogen atom to the main-chain nitrogen of residue 206 and the N6 nitrogen atom to Oδ1 of Asn175 and to the main-chain oxygen of residue 204. The N7 nitrogen atom finally is hydrogen bonded to the Nδ2 atom of Asn175.

The ribose part of the nucleotide forms only one hydrogen bond. The side chain of Glu211 interacts with the O2R hydroxyl. This residue is part of a loop region (residues 209−212) which in the free enzyme is flexible. In the binary complex with ADP, the electron density for these residues is considerably better defined, with clear density for the main chain and some of the side chains. Pro210, which folds over the adenine ring and forms hydrophobic interactions, and Glu211 are part of the ADP/ATP binding site, and their interactions with the nucleotide obviously stabilize the conformation of this part of the polypeptide chain.

The diphosphate group forms a number of hydrogen bonds to the enzyme, mainly with residues from the phosphate binding loop Gly8-X-X-X-X-X-Gly14-Lys15-Thr16. The conformation of this loop is, as can be seen from Figures 3 and 7, different from that observed in the native enzyme. Upon binding of the nucleotide, this part of the chain moves toward the active site so that the main-chain nitrogens of residues 12, 13, and 14 come close to the diphosphate group.

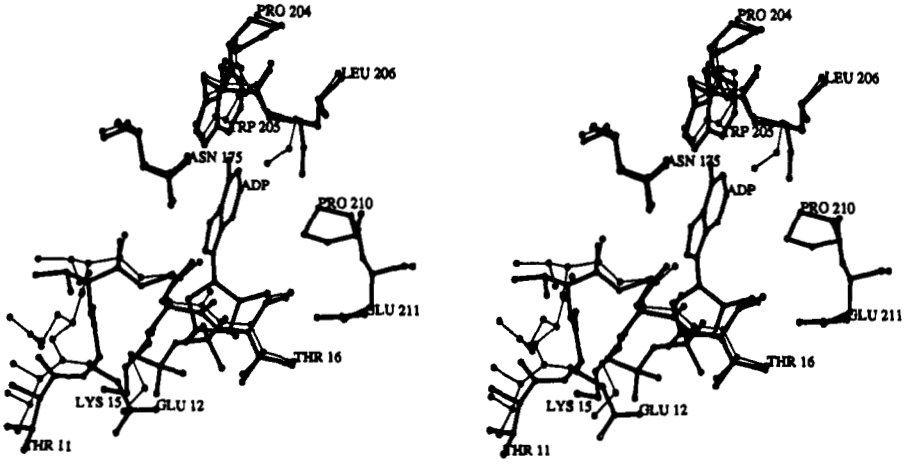

FIGURE 7: Stereoview of the ADP binding site in DTBS. The models of the native enzyme (thin lines) and the DTBS·ADP complex (thick lines) are superimposed.

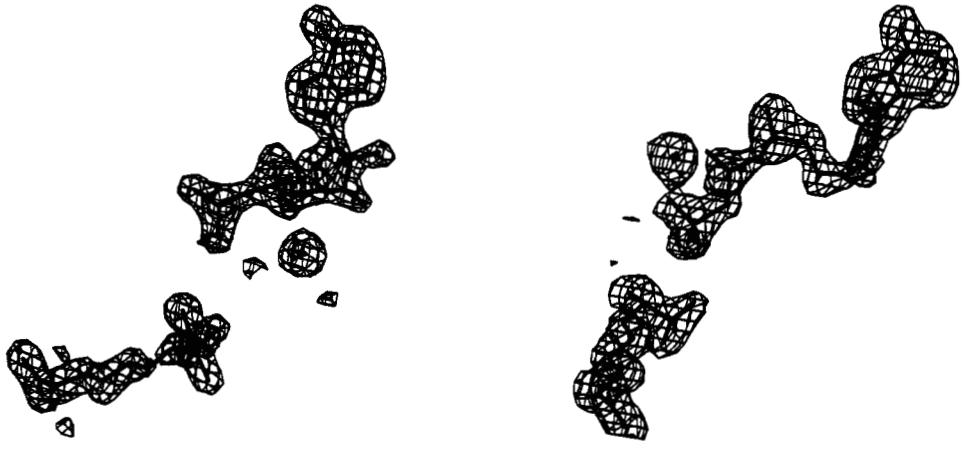

FIGURE 8: Difference electron density in the refined $|F_o| - |F_c|$ map for the bound substrates in quaternary complexes of DTBS. All substrate atoms and metal ions were excluded from the structure factor calculations. The electron density is contoured at the standard deviation of the electron density map. (a, left) DTBS·ADP·DAPA·Ca^{2+} complex; (b, right) DTBS·AMPPCP·DAPA·Mn^{2+} complex.

A large conformational difference is observed for the position of the side chain of Glu12, which instead of forming a salt bridge to Lys148 now points into the active site and is in the vicinity of the β-phosphate (3.4 Å).

The protein−phosphate interactions are mainly through main-chain hydrogen bonds; the β-phosphate group interacts with main-chain nitrogens of residues 15 and 16. One of the oxygens also forms a hydrogen bond to the $O\gamma$ of the Thr16 side chain and a solvent molecule. The phosphate bridging oxygen is hydrogen bonded to the main-chain nitrogen of residue 14. The α-phosphate group forms hydrogen bonds with main-chain nitrogens of residues 16 and 17, located in the first turn of helix α1. The second oxygen atom forms hydrogen bonds to two water molecules at the active site.

Enzyme·DAPA·ADP·Ca^{2+} Complex. The electron density for the substrate, ADP, and the Ca^{2+} ion is well defined in this quaternary complex (Figure 8a). Again, we find the strong additional electron density close to the N7 nitrogen atom of the substrate, which we interpret as the carboxyl group of the carbamate. The positions of DAPA and ADP are identical to the ones observed in the respective binary complexes, and the pattern of hydrogen bonding is essentially preserved.

There are slight structural changes in this complex when compared to the respective binary complexes. Due to the movement of the phosphate binding loop upon ADP binding, this loop is now closer to the substrate, compared to the binary enzyme·DAPA complex. As a consequence, the side chain of Glu12 is much closer (3.7 Å) to the N8 nitrogen atom of DAPA than in the DTBS·DAPA binary complex. Residue Thr11 has changed its side-chain conformation, and a new hydrogen bond from the $O\gamma$ atom to one of the carboxyl oxygen atoms of Glu12 is formed. In this ternary complex, we find very strong spherical electron density close to one oxygen of the α-phosphate at eight times of the rms deviation of the electron density map. We interpret this electron density as representing a Ca^{2+} ion. In addition to the phosphate oxygen of ADP, the side chain of Asp54 and four water molecules are found in the first coordination shell (<2.5 Å) of the metal ion resulting in approximately octahedral coordination geometry.

The phosphates of ADP are not in interacting distance with the carbamate. A water molecule is bridging the distance between an oxygen atom of the β-phosphate of ADP and one of the oxygens of the carbamate of DAPA.

Enzyme·AMPPCP·DAPA Complexes. In the refined model of the ternary complex enzyme·AMPPCP·DAPA, the binding mode and hydrogen-bonding pattern of DAPA and the ADP part of the ATP analog are identical to those observed in the complexes just described. The γ-phosphate group of the ATP analog is well defined in its electron density and is

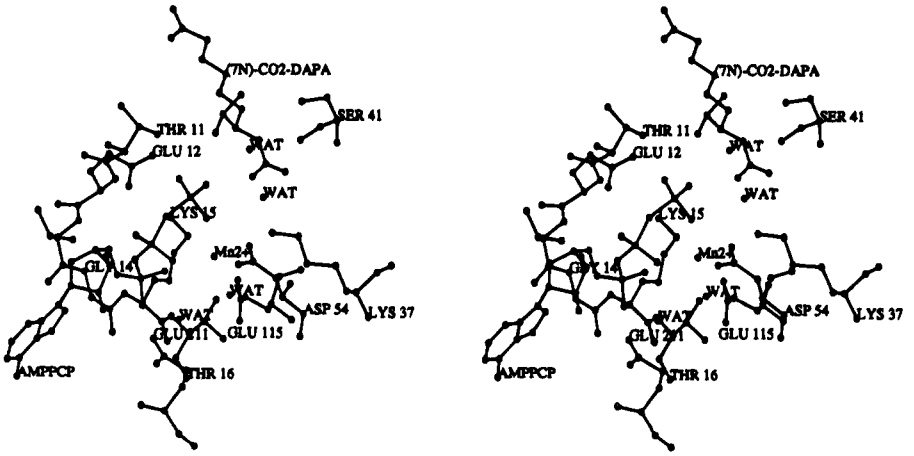

FIGURE 9: Stereoview of the active site of the enzyme in the quaternary complex DTBS·AMPPCP·DAPA·Mn^{2+}.

bound in the "giant anion hole" as defined by Dreusicke and Schulz (1986) close to the phosphate binding loop. The γ-phosphate bridges the space between the β-phosphate of the ADP and one of the oxygens of the carbamate so that this oxygen is pointing toward the phosphorus of the γ-phosphate group at a distance of 3.4 Å. Additional interactions of the γ-phosphate group are made through hydrogen bonds to the Oγ of the side chain of Thr11, the N8 nitrogen and one of the carbamate oxygens of DAPA, and two water molecules. The location and number of metal sites in the DTBS·AMPPCP·DAPA grown in the presence of $CaCl_2$ are not clear. Electron density was found at both the metal binding site observed in the DTBS·ADP·DAPA complex and at the expected binding position between the β- and γ-phosphate. However, the peak heights for these presumed metal ions are much less than in the DTBS·ADP·DAPA complex, which indicate replacement of the metal ion by water molecules. Also, the distances of these water molecules to the ligands are in the order of 2.7−3.0 Å, indicative of hydrogen bonds rather than coordination bonds. The position of the metal ion in the complex obtained in the presence of $MnCl_2$ is, however, very clear, and only one metal binding site was found (Figure 8b).[3] Figure 12 shows the Mn^{2+} bound to two oxygen atoms of the β- and γ-phosphate group. Protein ligands are the side chains of Asp54, Thr16, and Glu115. No indications for a manganese ion at the metal binding site observed in the DTBS·ADP·DAPA complex were found. Figure 9 shows a stereoview of the active site in the quaternary complex DTBS·AMPPCP·DAPA·Mn^{2+}.

It should be noted that the electron density for the carbamate in these complexes is less clear than in the binary complexes of enzyme with DAPA or in the ternary complex with ADP. In the complex obtained in the presence of Ca^{2+} ions, the carbamate density is found, albeit weaker. In the ternary complex grown in the presence of Mn^{2+}, the shape of the electron density corresponds to a DAPA molecule (Figure 8b), and no indication for the formation of a carbamate is found (the same batch of substrate, however, resulted in formation of the intermediate in crystals of the binary complex). One possible reason for the difficulty in forming the carbamate in the complex with the ATP analog can be inferred from the three-dimensional structure. The γ-phosphate group of AMPPCP is very close (approximately 3.4 Å) to the carboxyl group of the carbamate. This close proximity of two negative charges is not very favorable, and the additional phosphate group of the ATP analog disfavors the formation of the carbamate. The position of the γ-phosphate in the complex with the ATP analog is, however, about 0.3 Å closer to the carbamate than in the complex with ATP due to longer bond distances of the phosphorus atoms to the bridging carbon atom, and the charge repulsion in the catalytically competent complex might not be as pronounced.

There are differences between the interactions between the nucleotides and the protein described here and those reported in the paper by Alexeev et al. (1994b). On the basis of the sulfate positions in the native enzyme and an unrefined electron density map of a complex of DTBS with a nucleotide analog and the product, a model of the ATP binding site was proposed. The interactions of the ribose ring with the main-chain atoms of residues Thr16 and Val17 are not observed in our structure; Thr16 is bridging the $\alpha-\beta$ phosphate groups, and Val17 interacts with the α-phosphate of the nucleotide.

Comparison with Other Mononucleotide Binding Enzymes. As pointed out earlier (Huang et al., 1994), the mononucleotide binding motif of DTBS shares considerable similarities with another ATP-dependent enzyme, adenylate kinase. When our complexes are aligned with adenylate kinase complexed with its inhibitor Ap5A (Müller & Schulz, 1992), we found that the ATP binding site of these two enzymes does coincide (Figure 10a). In adenylate kinase, the adenosine ribose part of ATP is bound rather loosely, in contrast to the tight binding of the guanosine moiety of GTP in H-ras-p21 (Müller & Schulz, 1992). In DTBS, the adenosine ribose part forms tight interactions with the protein, and in this respect, as well as in the overall fold (Huang et al., 1994), the enzyme is more similar to the GTP binding H-ras-p21 protein than to the ATP binding adenylate kinase. The tight binding of the phosphates is well conserved in all three enzymes.

The GTP-dependent H-ras-p21 structure complexed with the slowly hydrolyzable GTP analog guanosine 5′-(β,γ-imido)triphosphate (Pai et al., 1990) shows surprising similarities to DTBS in mononucleotide binding. The

[3] DTBS complexes with Mn^{2+} are active in the presence of DAPA, CO_2, and ATP. With Mn^{2+} as the activating cation, the steady-state rate of dethiobiotin formation is about 6% of that observed in the presence of Mg^{2+}. Pre-steady-state experiments suggested that the major effect of Mn^{2+} was to slow the rate of dethiobiotin release from the enzyme (G. Lorimer, unpublished observations).

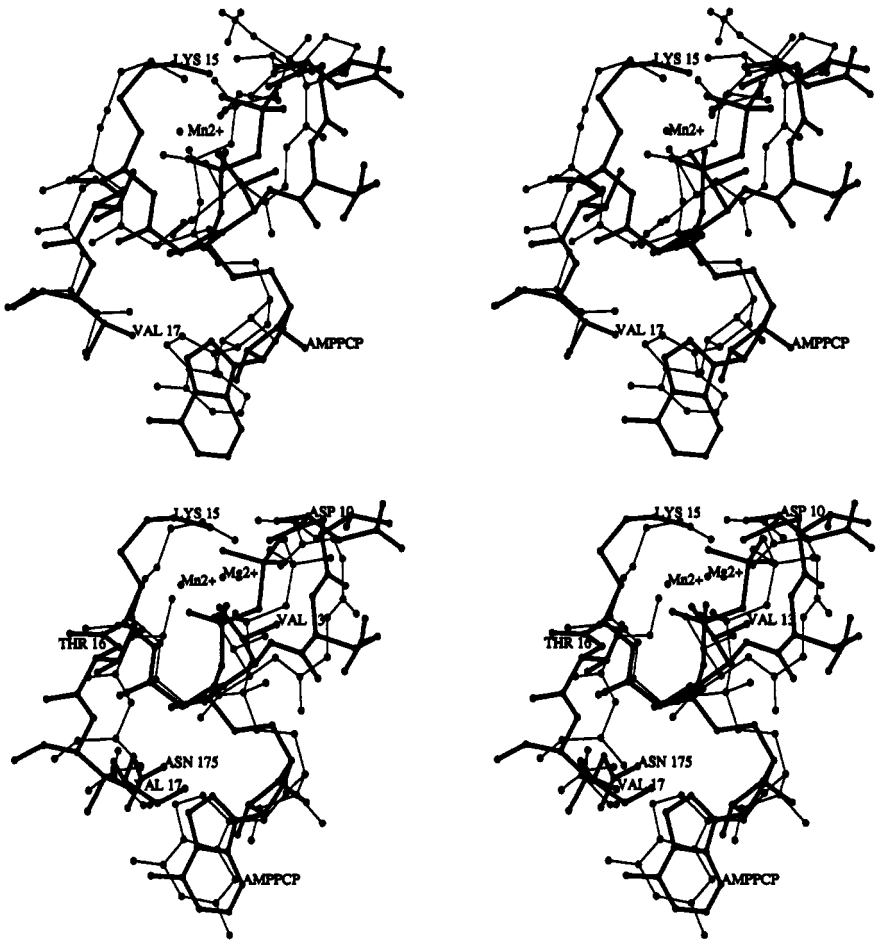

FIGURE 10: (a, top) Superposition of the nucleotide binding sites in DTBS (thick lines) and adenylate kinase (thin lines). (b, bottom) Superposition of the nucleotide binding sites in DTBS (thick lines) and p21-ras (thin lines).

nucleotides superimpose well when the two proteins are aligned (Figure 10b). Residue Asn175 which forms hydrogen bonds to the adenine ring is conserved and also forms one hydrogen bond to the base in H-ras-p21.

In spite of the fact that the phosphate binding loop in DTBS contains one more residue in the fingerprint region characteristic for this class of mononucleotide binding enzymes, many of the interactions of this loop with the phosphate group are conserved in the two enzymes. In the large anion hole, all main-chain nitrogens are pointing inward toward the phosphate, thereby creating a positively polarized local electrostatic field (Pai et al., 1990). The conserved residue Lys15 bridges two oxygen atoms from the β- and γ-phosphates. Thr16, which is conserved or conservatively substituted by a serine residue in this protein family, is bridging two α- and β-phosphate oxygens through hydrogen bonds.

The Mg^{2+} ion in H-ras-p21 is coordinated by the side chains of Ser17 and Thr35, two phosphate oxygens from the β- and γ- phosphate, respectively, and two water molecules. In DTBS, a metal ion is bound at the corresponding position with ligands from two oxygens of the phosphate groups of AMPPCP and the side chains of Asp54, Thr16, and Glu115.

In DTBS, there is, however, a second metal binding site, which at least in the complex with ADP and DAPA is clearly occupied. This metal site is located on the opposite site of the phosphate groups, toward the bulk solution. The metal binding site is formed by protein ligand Asp54, one oxygen atom from the α-phosphate, and surrounding water molecules (all distances being <2.5 Å). However, it is not clear whether this metal binding site is of functional significance.

Unlike ras-p21, there are few interactions between the ribose and DTBS. Only the side chain of Glu211 interacts with one of the hydroxyl groups, while in H-ras-p21, the carboxylic group of Asp30 forms interactions with both hydroxyl groups of the ribose, and the ring oxygen forms a hydrogen bond with Lys117.

DISCUSSION

The structure determination of binary, ternary, and quaternary complexes of DTBS has revealed the location of the active site and identified protein residues involved in binding of DAPA and nucleotide. Figure 11 provides a summary of the active site with the substrate and the ATP analog bound. For sake of simplicity, only those enzymic groups are included which might be of functional importance in catalysis. The active site of DTBS is located in a cleft formed between β-strands β1 and β4 and the connecting loops to adjacent α-helices α1 and α4. The reactive part of the substrate and the γ-phosphate group of the ATP analog reach into this cleft and are within interacting distance from each other. The cleft contains a cluster of polar conserved amino acids, which participate in binding of the nucleotide and DAPA molecules and which could also participate in the different catalytic steps. These enzymic groups are Thr11, Glu12, Lys15, Lys37, Ser41, and Asp54. The active

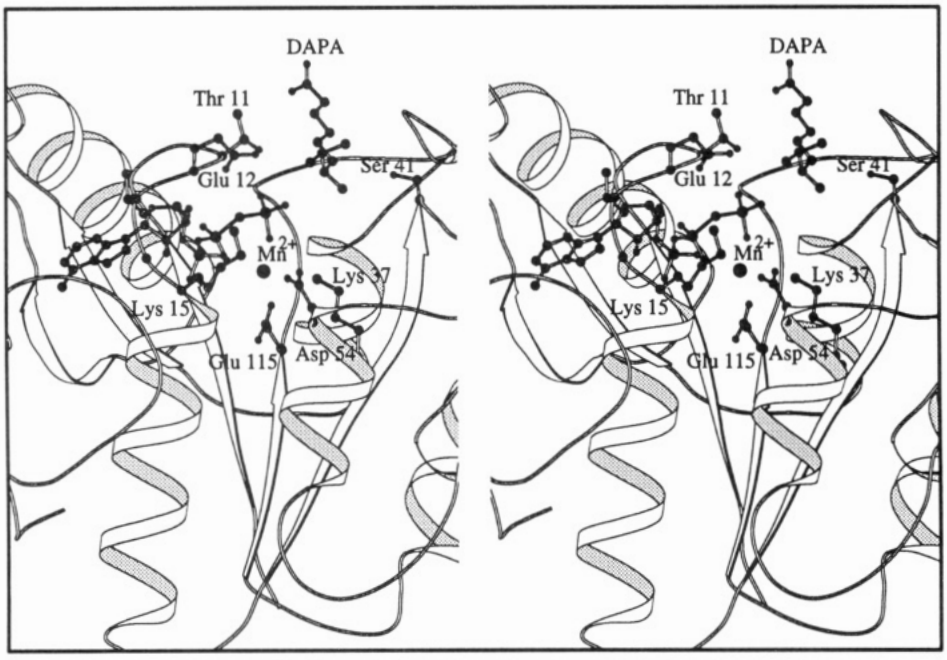

FIGURE 11: View of the active site of DTBS. Bound substrates and metal ions are included. Only enzymic groups with a potential role in catalysis are shown. The figure was generated with the program Molscript (Kraulis, 1991).

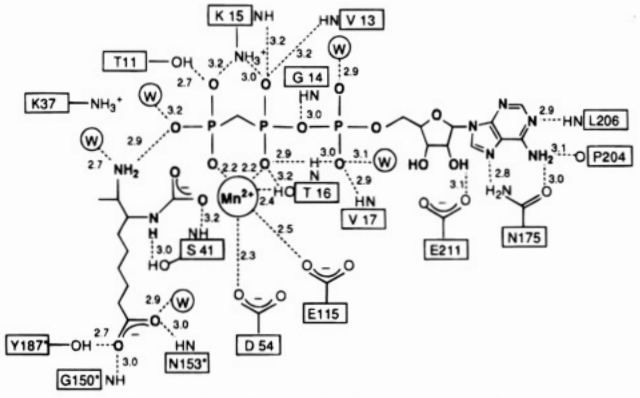

FIGURE 12: Schematic view of the interactions of AMPPCP and DAPA-$^{7N}CO_2$ with enzymic residues and the metal ion at the active site of DTBS. Protein residues from the second subunit are indicated by an asterisk. Hydrogen bonds (cutoff distance 3.2 Å) are indicated by dashed lines.

site is not completely shielded from the outer solution, and water molecules can reach the active center and might in fact participate as catalytic groups. Figure 12 gives a more detailed schematic view of the active site in the complex DTBS·AMPPCP·DAPA-$^{7N}CO_2$·Mn^{2+} composed from the structures of the complex DTBS·AMPPCP·DAPA grown in the absence and presence of Mn^{2+}.

The reaction catalyzed by DTBS can be divided into three consecutive bond making/breaking steps. The first step is the formation of the carbamate at one of the substrate nitrogens, followed by hydrolysis of ATP and formation of the second intermediate, the mixed carbamic−phosphoric anhydride. The last step of the reaction is ring closure with concomitant release of inorganic phosphate. This step of the reaction mechanism very likely proceeds through the formation of a tetrahedral intermediate formed upon nucleophilic attack of the 8-amino nitrogen on the carboxyl carbon atom of the carbamic−phosphoric anhydride. Figure 13 gives a minimal reaction mechanism, as can be deduced from the structures presented here.

One of the immediate questions which arises is why does the carbamate form in the crystals at rather low pH (6.5 in the crystallization mixture) and at low concentration of CO_2? Except for the complex DTBS·AMPPCP·DAPA, it forms stoichiometrically, since the occupancy at the active site of the carbamate group is as high as that of the other atoms of the substrate, as estimated from the height of the electron density and from a comparison to the structure of the DTBS·AEND complex.

The analysis of the enzyme complexes with the carbamylated substrate reveals that the carbamate is held in place through a number of tight interactions. Both carbamate oxygens form hydrogen bonds and salt bridges to enzymic groups. One of the oxygens forms a salt bridge with the side chain of Lys37 (3.3 Å distance) and also forms a hydrogen bond to a water molecule, which in turn is hydrogen bonded to the side chain of Lys15. The second oxygen atom of the carbamate forms a hydrogen bond to the main-chain nitrogen of Ser41.

The carbamate is partly buried in the protein and not totally accessible from the outside solution. The hydrogen bonds and, in particular, the two positive charges of the lysine residues can stabilize the carbamate sufficiently so that the reaction proceeds even at low concentrations of CO_2, providing an efficient trap for CO_2. Besides stabilizing the reaction intermediate, these enzymic groups could also facilitate the carbamylation step by polarizing the CO_2 molecule so that nucleophilic attack of the substrate nitrogen on the carbon atom can occur. The necessary proton abstraction from the N7 amino group could be mediated through a water molecule, either directly or via a proton relay system involving the side chain of Ser41 (Figure 13). Since no metal ions are bound to the enzyme in the absence of ADP or ATP, respectively, and the carbamate is formed in the absence of these nucleotides, it seems as if neither nucleotides nor the metal ions are involved in the carbamylation process. However, it has not yet been unambiguously shown whether this step is at all catalyzed by the enzyme.

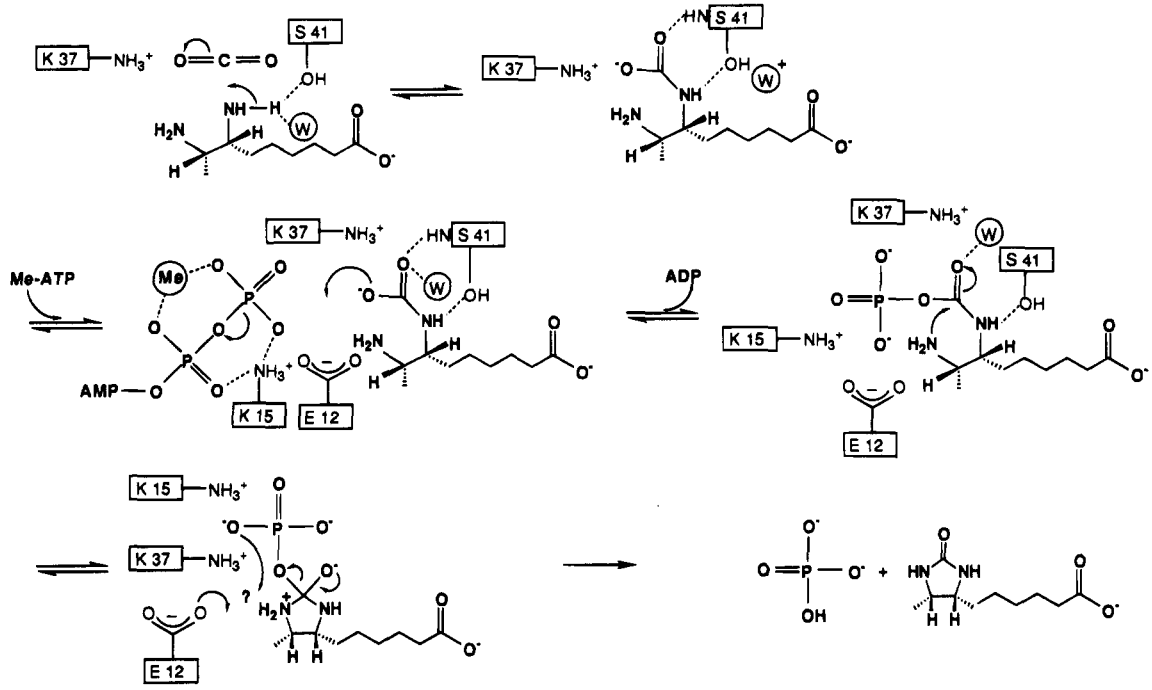

FIGURE 13: Minimal enzymatic reaction mechanism of dethiobiotin synthetase.

Since the DAPA carbamates are formed in solution, the enzyme might simply select for DAPA-$^{7N}CO_2$. Thus, DAPA-$^{7N}CO_2$ might not be the first reaction intermediate but the actual substrate.

The crystallographic identification of DAPA-$^{7N}CO_2$ as the enzyme-bound species is in contrast to earlier chemical trapping experiments (Baxter et al., 1994) which suggested the N8-carbamate as the reaction intermediate. The observed carbamate in our crystals very likely represents, however, a true intermediate on the reaction pathway of DTBS, since NMR and other studies also support carbamylation of DAPA at the N7 nitrogen atom (Gibson et al., 1995).

The next step of the catalytic reaction, the formation of the carbamic–phosphoric anhydride (Figure 13), can be envisaged from the complex of DTBS with DAPA and the nonhydrolyzable ATP analog. In this complex, one of the carbamate oxygen atoms is almost perfectly aligned for nucleophilic attack on the phosphorus atom of the γ-phosphate. The cleavage of the bond between the β- and γ-phosphate could be facilitated by protonation of the bridging oxygen atom. The only enzymic group close to the bridging oxygen is Glu12. However, the surroundings of Glu12 do not suggest an unusual pK_a for this residue, and it seems therefore unlikely that this group is involved in this step of the reaction mechanism.

The proposed mechanism for the subsequent steps in the enzymatic reaction, ring closure and release of inorganic phosphate, is not supported by direct structural evidence, since no structure with an analog of the carbamic–phosphoric anhydride intermediate is yet available. The following conclusions are therefore based on modeling studies. It is obvious from the three-dimensional structure of the DTBS·AMPPCP·DAPA complex that the diamino group of the substrate will have to shift its position when the carbamate attacks the phosphorus atom of the γ-phosphate group. The orientation and the alignment of the reactive carbon and nitrogen atom in the ring closure step can at present only be determined approximately, with the basic assumption that the phosphate group will maintain its position when the phosphorylated intermediate has been formed and the ADP has been released. Possible groups which might facilitate the nucleophilic attack of the N8 nitrogen atom on the activated carbonyl group are the side chain of Lys37, which could stabilize the negative charge developing at the carbonyl oxygen during nucleophilic attack and in the tetrahedral intermediate. After formation of this intermediate, the N8 nitrogen has to be deprotonated. One of the possible enzymic groups involved in this step might be Glu12, possibly through a proton-transfer system including Thr11. The subsequent cleavage of the carbon–oxygen bond could be accelerated by protonation of the bridging oxygen atom, resulting in a better leaving group. In a model of the phosphorylated intermediate–enzyme complex, there are no enzymic groups in the immediate vicinity of this oxygen which might act as a general acid, but water molecules at the active site could be possible proton donors. Protonation could be facilitated through a hydrogen bond network, involving a water molecule and the side chains of Thr11 and Glu12. However, it is also conceivable that one of the phosphate oxygens might abstract the proton from the N8 nitrogen atom directly, thereby neutralizing one of the negative charges.

The structurally related GTP-dependent enzyme adenylosuccinate synthetase (Huang et al., 1994; Alexeev et al., 1994b) has a similar step in its mechanism, where the substrate is phosphorylated by GTP during catalysis (Bass et al., 1984; Cooper et al., 1986). In this case, the γ-phosphate of GTP is transferred to the substrate IMP whereupon the amino group of the second substrate, L-aspartate, displaces the phosphate from its position by a nucleophilic attack on the C6 carbon of the intermediate. It is interesting to note that, in the structure of the unliganded enzyme (Poland et al., 1993), an acidic residue, Asp13, is located at the same position as Glu12 in DTBS. Furthermore, the positive charge of Lys37 in DTBS is conserved by Arg32 at the equivalent position in the 3D structure of

the synthetase. The conservative replacement of these side chains might indicate similar functions in the reaction mechanism of the two enzymes.

Phosphotransferases in general seem to require a divalent cation complexed to phosphoryl oxygen atoms. A number of functions for the metal ion have been suggested, such as (1) compensating the negative charge on the γ-phosphate, thereby facilitating nucleophilic attack on the phosphorus atom, (2) binding to the α- and β-phosphates of ADP, making it a better leaving group, (3) acting as template to place the oligophosphate with respect to other catalytic groups, (4) stabilization of the transition state, and (5) holding the nucleophile in place for phosphoryl transfer (Coopermann, 1976; Knowles, 1980; Herschlag & Jencks, 1990). While the metal ion can fulfill one or several of these roles, its precise function may be different in the various enzymes, given their mechanistic and structural diversity, in particular, the observed differences in the ligation states of the metal ion. In DTBS, one function of the metal ion is very likely to neutralize the negative charges on the γ-phosphate, together with the N8 nitrogen of DAPA, the side chain of Lys15, and the surrounding main-chain amino nitrogens. The metal ion might also be required to properly position the phosphate groups. There are no direct interactions between the metal ion and the nucleophile, the carbamate group of DAPA. Due to the distance between the metal ion and the closest carbamate oxygen of 4.8 Å, a role of the metal ion in positioning the nucleophile for phosphoryl transfer thus seems unlikely.

ACKNOWLEDGMENT

We thank Dr. George Lorimer for critical comments on the manuscript, Dr. Barry Wexler for the samples of DAPA, and Ivan Turner, Hongji Chi, and Eileen Marsilii for technical assistance.

REFERENCES

Alexeev, D., Bury, S. M., Boys, C. W. G., Turner, M. A., Sawyer, L., Ramsey, A. J., Baxter, H. C., & Baxter, R. L. (1994a) *J. Mol. Biol. 235*, 774−776.

Alexeev, D., Baxter, R. L. & Sawyer, L. (1994b) *Structure 2*, 1061−1072.

Bass, M. B., Fromm, H. J., & Rudolph, F. B. (1984) *J. Biol. Chem. 259*, 12330−12333.

Baxter, R. L., & Baxter, H. C. (1994) *J. Chem. Soc. Commun.*, 759−760.

Baxter, R. L., Ramsey, A. J., Mclver, L. A., & Baxter, H. C. (1994) *J. Chem. Soc. Commun*, 559−560.

Blum, M., Metcalf, P., Harrison, S. C., & Wiley, D. C. (1987) *J. Appl. Crystallogr. 20*, 235−242.

Brünger, A. T., Kuriyan, J., & Karplus, M. (1987) *Science 235*, 458−460.

Collaborative Computational Project, Number 4, (1994) *Acta Crystallogr. D50*, 760−763.

Cooper, B. F., Fromm, H. J., & Rudolph, F. B. (1986) *Biochemistry 25*, 7323−7327.

Cooperman, B. S. (1976) in *Metal Ions in Biological Systems* (Sigel, H., Ed.) Vol. 5, pp 79−125, Marcel Dekker, New York.

Dreusicke, G., & Schulz, G. E. (1986) *FEBS Lett. 208*, 301−304.

Gibson, K. J., Lorimer, G. H., Rendina, A. R., Taylor, W. S., Cohen, G., Gatenby, A. A., Payne, W. G., Roe, D. C., Lockett, B. A., Nudelman, A., Marcovici, D., Nachum, A., Wexler, B. A., Marsilii, E. L., Turner, I. M., Sr., Howe, L. D., Kallbach, C. E., & Chi, H. (1995) *Biochemistry 34*, 10976−10984.

Glöckler, R., Ohsawa, I., Speck, D., Ledoux, C., Bernard, S., Zinsius, M., Villeval, D., Kisou, T. Kamogawa, K., & Lemoine, Y. (1990) *Gene 87*, 63−70.

Hatakayema, K., Hohama, K., Verttes, A. A., Kobayashi, M., Kurusu, Y., & Yukawa, H. (1994) *DNA Sequence 4*, 177−184.

Herschlag, D., & Jencks, W. P. (1990) *Biochemistry 29*, 5272−5170.

Huang, W., Lindqvist, Y., Schneider, G., Gibson, K. J., Flint, D., & Lorimer, G. *Structure 2*, 407−414.

Jones, T. A., Zou, J., Cowan, S., & Kjeldgaard, M. (1991) *Acta Crystallogr. A47*, 110−119 .

Knowles, J. R. (1980) *Annu. Rev. Biochem. 49*, 877−919.

Kraulis, P. (1991). *J. Appl. Crystallogr. 24*, 946−950.

Krell, K., & Eisenberg, M. A. (1970) *J. Biol. Chem.245*, 6558−6586.

Laskowski, R. A., McArthur, M. W., Moss, D. S., & Thornton, J. M. (1993) *J. Appl. Crystallogr. 26*, 282−291.

Müller C. W., & Schulz, G. E. (1991) *J. Mol. Biol. 224*, 159−177.

Pai, E. F., Krengel, U., Petsko, G. A., Goody, R. S., Kabsch, W., & Wittinghofer, A. (1990) *EMBO J. 9*, 2351−2359.

Poland, B. W., Silva, M. M., Serra, M. A., Cho, Y., Kim, K. H., Harris, E. M. S., & Honzatko, R. B. (1993) *J. Biol. Chem. 268*, 25334−25342.

Sakurai, N. (1993) GENEMBL accession number D17468.

Sato, M., Yamamoto, M., Imada, K., & Katssube, Y. J. (1992) *J. Appl. Crystallogr. 25*, 348−357.

BI9505934